Applied Physics Letters

Spin-orbit-torque-driven multilevel switching in Ta/CoFeB/MgO structures without initialization

Cite as: Appl. Phys. Lett. **114**, 042401 (2019); https://doi.org/10.1063/1.5079313
Submitted: 30 October 2018 • Accepted: 13 January 2019 • Published Online: 29 January 2019

S. Zhang, Y. Su, X. Li, et al.

View Online

Export Citation

CrossMark

ARTICLES YOU MAY BE INTERESTED IN

Spin transfer torque devices utilizing the giant spin Hall effect of tungsten
Applied Physics Letters **101**, 122404 (2012); https://doi.org/10.1063/1.4753947

Spin-orbit torques: Materials, physics, and devices
Applied Physics Letters **118**, 120502 (2021); https://doi.org/10.1063/5.0039147

Field-free spin-orbit torque switching of a perpendicular ferromagnet with Dzyaloshinskii-Moriya interaction
Applied Physics Letters **114**, 022401 (2019); https://doi.org/10.1063/1.5052194

© 2019 Author(s).

Spin-orbit-torque-driven multilevel switching in Ta/CoFeB/MgO structures without initialization

Cite as: Appl. Phys. Lett. **114**, 042401 (2019); doi: 10.1063/1.5079313
Submitted: 30 October 2018 · Accepted: 13 January 2019 · Published Online: 29 January 2019

S. Zhang,[a)] Y. Su,[a)] X. Li, R. Li, W. Tian, J. Hong, and L. You[b)]

AFFILIATIONS

School of Optical and Electronic Information, Huazhong University of Science and Technology, Wuhan 430074, China

[a)] **Contributions:** S. Zhang and Y. Su contributed equally to this work.
[b)] **Author to whom correspondence should be addressed:** lyou@hust.edu.cn

ABSTRACT

Spin-orbit torque (SOT) has been proposed as an alternative writing mechanism for the next-generation magnetic random access memory (MRAM), due to its energy efficiency and high endurance in perpendicular magnetic anisotropic materials. However, the three-terminal structure of SOT-MRAM increases the cell size and consequently limits the feasibility of implementing high density memory. Multilevel storage is a key factor in the competitiveness of SOT-MRAM technology in the nonvolatile memory market. This paper presents an experimental characterization of a multilevel SOT-MRAM cell based on a perpendicularly magnetized Ta/CoFeB/MgO heterostructure and addresses the initialization-free issue of multilevel storage schemes. Magneto-optical Kerr effect microscopy and micromagnetic simulation studies confirm that the multilevel magnetization states are created by changing a longitudinal domain wall pinning site in the magnet. The realization of robust intermediate switching levels in the commonly used perpendicularly magnetized Ta/CoFeB/MgO heterostructure provides an efficient way to switch magnets for low-power, high-endurance, and high-density memory applications.

Published under license by AIP Publishing. https://doi.org/10.1063/1.5079313

The conventional spin-transfer torque magnetic random access memory (STT-MRAM) offers non-volatility, high densities, and complementary metal-oxide semiconductor (CMOS) process compatibility.[1–4] However, the key drawback of STT-MRAM is that reading and writing current share the same path through the junction.[3–6] Hence, the aging of the tunnel barrier is accelerated on injecting high-write-current densities, especially for switching on the nanosecond time scale. Moreover, the read disturb challenge grows with the scaling technology as the read-to-write current ratio decreases. Fortunately, the concept of a three-terminal magnetic memory device based on a spin-orbit torque (SOT) effect has been recently proposed in heavy metal (HM)/ferromagnetic metal (FM)/oxide heterostructures, where the magnetic bit is written by a current pulse injected through the bottom HM, and a magnetic tunnel junction (MTJ) can be employed to read the state of the magnetic bit, namely, the SOT-MRAM.[3,4,7–11] The decoupled write and read paths of SOT devices can naturally resolve the problems related to the endurance and reliability of conventional two-terminal STT-MRAMs. Moreover, separate optimization is available for tuning the two independent read and write channels, relaxing the high magnetoresistance ratio and low resistance-area product simultaneously required for MRAM.

However, the low storage density problem in a SOT-MRAM becomes serious owing to its three-terminal architecture. One key solution is the multilevel cell (MLC) configuration, a mature technique already utilized in flash memories, which can provide an enhanced integration density. Until now, the demonstration of MLC in SOT-MRAM has been rarely reported. Four-bit SOT-MLC was demonstrated by connecting two MTJs in one storage element.[12] However, the fabrication process of such a design is complicated. Recently, SOT-MLC design was reported in a Co/Pt multilayer ferromagnet by controlling the multidomain formation through the current pulse and also in Pt/Co/Ta/Co multilayers by tilting the magnetization through an external magnetic field or antiferromagnetic interlayer coupling.[13–16] By contrast, from the material point of view, materials such as CoFeB which combine high spin polarization and a low Gilbert damping constant are highly desirable for spintronic devices. In addition, Ta/CoFeB/MgO heterostructures with perpendicular magnetic anisotropy offer high scalability as the shape anisotropy field

effect is negligible and have been commonly used in perpendicular MTJ with high tunnel magnetoresistance.[2,17,18]

Here, we report that multilevel magnetization states can be controlled in perpendicularly magnetized Ta/CoFeB/MgO heterostructures by modulating the in-plane field and are independent of the initial state. The film stack consists of Ta (10 nm)/$Co_{40}Fe_{40}B_{20}$ (CoFeB, 1.2 nm)/MgO (1.6 nm)/Ta (20 nm) (from the bottom), which is sputtered on a thermally oxidized Si substrate at room temperature. This heterostructure closely resembles the one described in our previous work.[19] As depicted in Fig. 1(a), when an in-plane charge current flows through the Ta layer, the spin current is generated due to the spin Hall effect (SHE) in Ta and is transmitted across the Ta/CoFeB interface. This results in the application of a torque on the CoFeB layer. The devices based on such a heterostructure are patterned into a Hall bar with dimensions of 400 (length) × 50 (width) μm^2 [Fig. 1(b)]. The anomalous Hall resistance R_H, which is proportional to the average out-of-plane magnetization component of CoFeB, is measured under a small current of 0.1 mA. Measurements as a function of a vertical magnetic field exhibit sharp switching, indicating a good perpendicular magnetic anisotropy (PMA) in the cells [Fig. 1(c)]. Current-induced switching is measured by applying a current pulse (0.5 s in duration) under the assistance of an in-plane magnetic field H_x collinear to the current. With a fixed magnetic field in the +x direction, sweeping a quasistatic in-plane current generates hysteretic magnetic switching between the $M_z > 0$ and $M_z < 0$ states, with the positive current favoring $M_z > 0$ [Fig. 1(d)]. The switching direction changes when the in-plane field is inversed. This is consistent with negative spin Hall angle θ_{SH} in Ta, which was reported to be −0.09 in our previous work.[19]

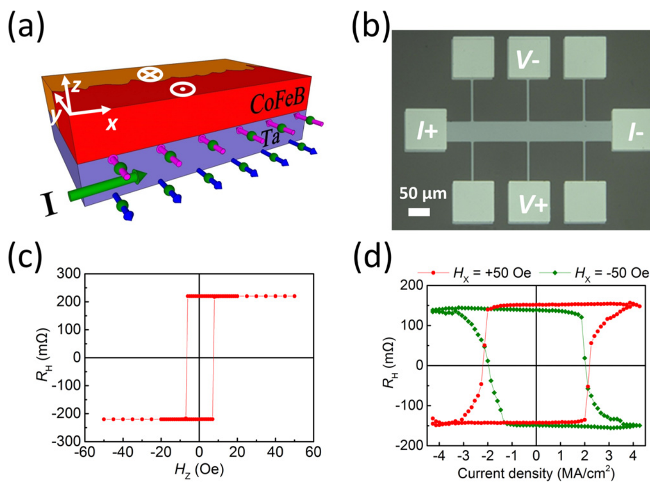

FIG. 1. SHE-driven magnetization switching. (a) Sample geometry for SHE switching measurements. In-plane current flowing through tantalum along the x direction (electrons along the –x direction) causes spin separation across the thickness of the tantalum (z-direction). This results in the accumulation of electrons with y-polarized spins at the Ta/CoFeB interface, which offers SHE-induced spin torque to the magnetization and thereby moves the domain wall with the assistance of the in-plane magnetic field H_x. I represents the applied direct current, and the green arrow denotes the current direction. The blue and pink arrows represent the orientations of accumulated spins. The red and orange colors in the CoFeB film indicate the magnetic domains with opposite directions of magnetic moments, which is either "upwards" or "downwards". (b) Optical micrograph of the fabricated Hall bar structure. The width of the Hall bar (W) is 50 μm, and the length (L) is 400 μm. (c) Anomalous Hall resistance R_H as a function of the perpendicular magnetic field H_z (R_H-H_z loop). (d) Current-induced magnetization reversal when H_x is parallel (red) or antiparallel (green) to the current direction.

According to SHE, when the charge current flows along x, the spin moments within the generated spin current point in the y direction. The effective magnetic field produced by SOT can be expressed as $\vec{H}^{SOT} \propto \vec{M} \times y$. As a result, the z-component of the SOT effective field, H_z^{SOT}, is expressed as[8]

$$H_z^{SOT} = \frac{\hbar}{2eM_s t}\theta_{SH} J\, m_x, \tag{1}$$

where $\hbar$ is Planck's constant, e is the electron charge, M_s is the saturation magnetization, t is the thickness of the CoFeB layer, θ_{SH} is the spin Hall angle of Ta, and J is the current density. It is reported that the function of the in-plane magnetic field H_x is to orient the magnetic moments within the domain wall (DW) to have a significant in-plane component m_x.[20] Therefore, a tunable effective field H_z^{SOT} can be exerted on the magnetic film by varying the magnitude and the direction of H_x. Hence, the domain configuration and the resultant Hall resistances of the Hall bar can be controlled by varying the external magnetic field H_x.

This concept is confirmed by our measurement of R_H–J loops under various H_x, as depicted in Fig. 2. Under the in-plane magnetic field of abs(H_x) < 20 Oe, the magnetization switching is incomplete and results in an R_H value smaller than the value at $H_x = \pm 20$ Oe. In addition, the magnetization switching even starts to occur at the very small in-plane field abs(H_x) ≤ 2 Oe, which indicates that DW could move under a small SOT effective field H_z^{SOT} in our film structure. This magnetic field range (2–20 Oe) along with the switching current density (<3.5×10^6 A cm^{-2}) is lower than the reported value in similar Ta/CoFeB/MgO structures.[21,22] With an H_x larger than 20 Oe, for instance, when H_x = 50Oe, 100Oe, and 200 Oe, there is no significant change in the R_H value (see Sec. S1 of the supplementary material). By analyzing the dependence of the SOT efficiency on the in-plane field, a Dzyaloshinskii–Moriya interaction (DMI) effective field (H_{DMI}) is obtained to be around 100 Oe (referring to Sec. S2 of the supplementary material), stabilizing a right handed Néel wall of the ferromagnet. The DMI constant was estimated to be around 0.13 mJ m^{-2}, which is close to the reported values in similar structures.[21,23]

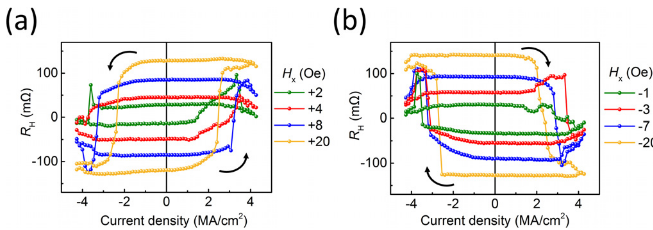

FIG. 2. R_H-J loops measured under different values of (a) positive and (b) negative in-plane magnetic fields H_x.

Published under license by AIP Publishing

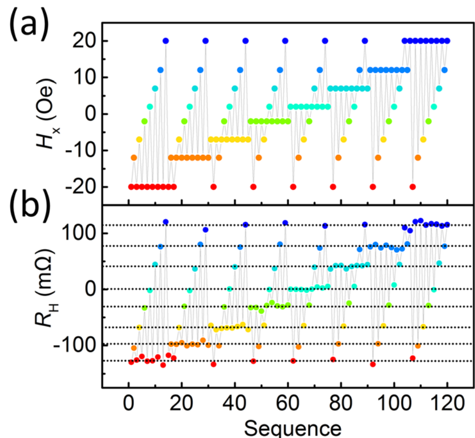

FIG. 3. Multilevel states in the Ta/CoFeB/MgO heterostructure controlled by eight different in-plane magnetic fields H_x under a current with a current density of $J = 4.3 \times 10^6$ A cm^{-2}. (a) Sequence of applied magnetic fields H_x. (b) Corresponding R_H response to the H_x sequence shown in (a).

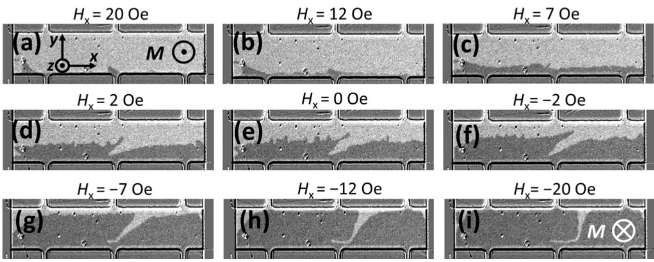

FIG. 4. MOKE microscopy images of a Hall bar device after applying a series of external magnetic fields H_x: from (a) 20 Oe to (i) −20 Oe in the presence of a current pulse with an amplitude of $J = 3.5 \times 10^6$ A cm^{-2} and a duration of 0.5 s along the +x direction. Bright and dark regions in the channel correspond to magnetization pointing upward ($+m_z$) and downward ($-m_z$), respectively.

In most multilevel storage mechanisms, extra initialization steps are required to reset the memory cell for the next writing event.[24–26] This results in a prolonged writing time and increased power consumption. MLC design using an SOT mechanism in Co/Pt multilayers resolves this issue.[13] Here, we also emphasize that the initialization is no longer necessary in our MLC scheme. As shown in Fig. 3, by applying different values of the magnetic field H_x such as ±20, ±12, ±7, and ±2 Oe, the MLC can be set to eight resistance states at a fixed current density of $J = 4.3 \times 10^6$ A cm^{-2}. The Hall resistance solely relies on the H_x value and does not rely on the previous magnetic states. In such a scheme, the state can be written to a target level from any of the eight levels, and it can also reach all other levels from one particular level. This means that any of the multistates can be achieved by setting the corresponding in-plane magnetic field without any initialization step. Here, the demonstrated eight Hall resistance states can represent an MLC with 8 bits. The multilevel states hint that the evolution of domain structures must play an important role.

The domain configurations can be visualized by using Magneto-optical Kerr effect (MOKE) spectroscopy, as shown in Fig. 4. We saturated the magnetization M (pointing downwards) in the Hall bar by using a sufficiently high external field and then applied a current pulse ($J = 3.5 \times 10^6$ A cm^{-2} in current density and 0.5 s in duration) along the +x direction in the presence of different magnitudes of the in-plane magnetic field H_x. Under H_x = 20 Oe, most of the magnetic moments were reversed to point upwards [Fig. 4(a)]. Then, H_x swept to −20 Oe step by step, and the MOKE images were captured at every step, as shown in Figs. 4(b)–4(i). It can be seen clearly that the pinning site of the longitudinal domain wall depends on the magnitude of H_x. The magnetization orientation in the reversed domain was determined by the z component of the Oersted field generated by the current pulse (a detailed analysis can be found in Sec. S3 in the supplementary material). By reversing the direction of the current, the position of the $m_z = 1$ and $m_z = -1$ polarized domains was reversed (referring to Sec. S4 of the supplementary material).

As a complementary confirmation, we also performed Object-Oriented Micro-Magnetic Framework (OOMMF) micromagnetic simulations (details can be found in Sec. S5 in the supplementary material) based on the generalized Landau–Lifschitz–Gilbert (LLG) theory in order to obtain the relationship between H_x and the DW pinning position.[27] Through the micromagnetic simulations, the controlling of DW displacement by the in-plane field and an initialization-free process are demonstrated. As shown in Fig. 5(a), with out-of-plane Oersted fields acting on the top and bottom edges and an in-plane current flowing through the whole magnet simultaneously, 7 different magnitudes of in-plane fields induce 7 stable magnetization states of the magnet. Then, an identical in-plane field of −200 Oe is applied on the magnet with the aforementioned 7 initial states. We observe that whatever the initial state be, the same final state is obtained under an identical in-plane field [Fig. 5(b)]. That is to say, in our multilevel cell device, final states are only controlled by the in-plane field, and no initialization is needed in the working process. The simulations show qualitative agreement with our experimental results except the larger in-plane fields used in simulations. The main reason for such

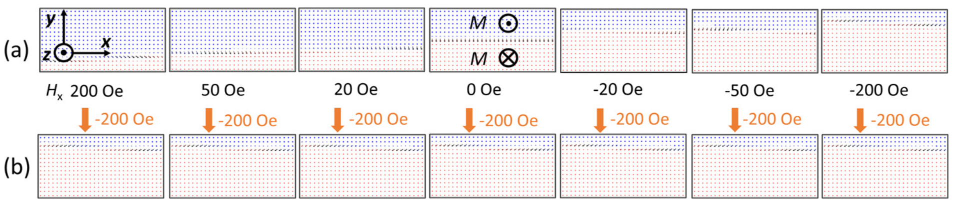

FIG. 5. Micromagnetic simulations of initialization-free switching with the Oersted field and SOT acting on the magnet. (a) The various initial states achieved under different in-plane fields. (b) The corresponding final states when the in-plane field switches to −200 Oe.

Published under license by AIP Publishing

discrepancy is the imperfection of real material structures, and the temperature has not been taken into account in simulation.

In Fig. 5(a), the arrows in the DW represent the direction of magnetization moments. It is clearly shown that in the presence of the in-plane magnetic field, the magnetic moment inside the DW prefers to align with the external field. The magnitude of H_x determines the tilting angle of the magnetic moments within the DW. As a result, according to Eq. (1), perpendicular SOT effective fields are different under various in-plane fields. For our CoFeB film considered here, the longitudinal DW is likely to be of Néel-type due to the DMI effective field, as previously mentioned. In the case of $H_x = 0$, H_z^{SOT} is zero as $m_x = 0$ within the DW. The DW finally displaces to the center of the Hall bar under the combined effect of the Oersted field, DMI field, exchange field, magnetostatic field, etc., in accordance with $R_H = 0\,\Omega$. However, for $H_x \neq 0$, H_z^{SOT} drives the DW, moving it to a new pinning position and resulting in an intermediate magnetization between full saturation and demagnetization. The DW pinning effect is preferred to lower the total energy. The final steady position of the DW depends on the orientation and magnitude of H_z^{SOT}.

In our demonstration, in principle, the pinned position of the longitudinal DW, and consequently anomalous Hall effect resistance, can be tuned in an analogue manner by magnetic fields, which indicates that our devices may exhibit a memristive behavior. On the other hand, to confirm the feasibility of scaling down, we performed OOMMF micromagnetic simulations with the cell size down to $80 \times 80\,\mathrm{nm}^2$, which still resulted in dual magnetic domains. It is possible to approach MLCs below 100 nm by carefully adjusting the material properties. Consequently, our devices can be used as artificial synapses in artificial neural networks for neuromorphic computing.[28] Besides, due to the large memory capacity, MLC may become a good candidate for processing-in-memory.[29]

In summary, we investigated that multilevel resistance states can be achieved in the perpendicularly magnetized Ta/CoFeB/MgO heterostructure by controlling the magnetization configurations of the magnet through an in-plane magnetic field. The DW moves orthogonally to the current flow driven by SOT, and the final pinning position of the DW is independent of its initial state. These results are crucial in the realization of high-density and low-power-consumption SOT-MRAM and ferromagnetic memristor applications.

See supplementary material for current induced switching under in-plane fields above 20 Oe (S1), the estimation of the DMI constant (S2), the analysis of Oersted field inducing nucleation (S3), MOKE images under current along the −x direction (S4), and details of OOMMF micromagnetic simulations (S5).

This work was financially supported by the National Natural Science Foundation of China (NSFC Grant Nos. 61674062 and 61821003).

REFERENCES

[1] S. A. Wolf, D. D. Awschalom, R. A. Buhrman, J. M. Daughton, S. von Molnár, M. L. Roukes, A. Y. Chtchelkanova, and D. M. Treger, Science **294**, 1488 (2001).

[2] S. Ikeda, K. Miura, H. Yamamoto, K. Mizunuma, H. D. Gan, M. Endo, S. Kanai, J. Hayakawa, F. Matsukura, and H. Ohno, Nat. Mater. **9**, 721 (2010).

[3] A. D. Kent and D. C. Worledge, Nat. Nanotechnol. **10**, 187 (2015).

[4] S. Bhatti, R. Sbiaa, A. Hirohata, H. Ohno, S. Fukami, and S. N. Piramanayagam, Mater. Today **20**, 530 (2017).

[5] W. S. Zhao, Y. Zhang, T. Devolder, J. O. Klein, D. Ravelosona, C. Chappert, and P. Mazoyer, Microelectron. Reliab. **52**, 1848 (2012).

[6] Z. Diao, Z. Li, S. Wang, Y. Ding, A. Panchula, E. Chen, L.-C. Wang, and Y. Huai, J. Phys.: Condens. Matter **19**, 165209 (2007).

[7] L. Liu, C.-F. Pai, Y. Li, H. W. Tseng, D. C. Ralph, and R. A. Buhrman, Science **336**, 555 (2012).

[8] L. Liu, O. J. Lee, T. J. Gudmundsen, D. C. Ralph, and R. A. Buhrman, Phys. Rev. Lett. **109**, 096602 (2012).

[9] K. Cai, M. Yang, H. Ju, S. Wang, Y. Ji, B. Li, K. W. Edmonds, Y. Sheng, B. Zhang, N. Zhang, S. Liu, H. Zheng, and K. Wang, Nat. Mater. **16**, 712 (2017).

[10] R. Bishnoi, M. Ebrahimi, F. Oboril, and M. B. Tahoori, in *19th Asia South Pacific Design Automation Conference* (ASP-DAC) (SunTec, Singapore, 2014), p. 1.

[11] G. Prenat, K. Jabeur, G. Di Pendina, O. Boulle, and G. Gaudin, in *Spintronics-Based Computing*, edited by W. Zhao and G. Prenat (Springer, Berlin, 2015), pp. 145–157.

[12] Y. Kim, X. Fong, K.-W. Kwon, M.-C. Chen, and K. Roy, IEEE Trans. Electron Devices **62**, 561 (2015).

[13] K.-F. Huang, D.-S. Wang, M.-H. Tsai, H.-H. Lin, and C.-H. Lai, Adv. Mater. **29**, 1601575 (2017).

[14] Y. Sheng, Y. C. Li, X. Q. Ma, and K. Y. Wang, Appl. Phys. Lett. **113**, 112406 (2018).

[15] Y. Sheng, K. W. Edmonds, X. Ma, H. Zheng, and K. Wang, Adv. Electron. Mater. **4**, 1800224 (2018).

[16] Y. Cao, A. Rushforth, Y. Sheng, H. Zheng, and K. Wang, e-print arXiv:1810.09064.

[17] D. C. Worledge, G. Hu, D. W. Abraham, J. Z. Sun, P. L. Trouilloud, J. Nowak, S. Brown, M. C. Gaidis, E. J. O'Sullivan, and R. P. Robertazzi, Appl. Phys. Lett. **98**, 022501 (2011).

[18] H. Sato, E. C. I. Enobio, M. Yamanouchi, S. Ikeda, S. Fukami, S. Kanai, F. Matsukura, and H. Ohno, Appl. Phys. Lett. **105**, 062403 (2014).

[19] L. You, O. J. Lee, D. Bhowmik, D. Labanowski, J. Hong, J. Bokor, and S. Salahuddin, Proc. Natl. Acad. Sci. U. S. A. **112**, 10310 (2015).

[20] O. J. Lee, L. Q. Liu, C. F. Pai, Y. Li, H. W. Tseng, P. G. Gowtham, J. P. Park, D. C. Ralph, and R. A. Buhrman, Phys. Rev. B **89**, 024418 (2014).

[21] J. Cao, Y. Chen, T. Jin, W. Gan, Y. Wang, Y. Zheng, H. Lv, S. Cardoso, D. Wei, and W. S. Lew, Sci. Rep. **8**, 1355 (2018).

[22] D. Bhowmik, M. E. Nowakowski, L. You, O. Lee, D. Keating, M. Wong, J. Bokor, and S. Salahuddin, Sci. Rep. **5**, 11823 (2015).

[23] J. Torrejon, J. Kim, J. Sinha, S. Mitani, M. Hayashi, M. Yamanouchi, and H. Ohno, Nat. Commun. **5**, 4655 (2014).

[24] N. Papandreou, A. Pantazi, A. Sebastian, M. Breitwisch, C. Lam, H. Pozidis, and E. Eleftheriou, in *Proceedings of IEEE International Conference on Electronics Circuits Systems* (ICECS) (IEEE, Piscataway, Athens, Greece, 2010), p. 1017.

[25] M. Wuttig and N. Yamada, Nat. Mater. **6**, 824 (2007).

[26] Y. Chen, W.-F. Wong, H. Li, C.-K. Koh, Y. Zhang, and W. Wen, J. Emerging Technol. Comput. Syst. **9**, 16 (2013).

[27] M. J. Donahue and D. G. Porter, "Oommf user's guide, version 1.0," Interagency Report No. NIST IR 6376, National Institute of Standards and Technology, Gaithersburg, MD, USA, 1999.

[28] P. A. Merolla, J. V. Arthur, R. Alvarez-Icaza, A. S. Cassidy, J. Sawada, F. Akopyan, B. L. Jackson, N. Imam, C. Guo, Y. Nakamura, B. Brezzo, I. Vo, S. K. Esser, R. Appuswamy, B. Taba, A. Amir, M. D. Flickner, W. P. Risk, R. Manohar, and D. S. Modha, Science **345**, 668 (2014).

[29] J. Ahn, S. Hong, S. Yoo, O. Mutlu, and K. Choi, ACM SIGARCH Comput. Archit. News **43**, 105 (2016).

Published under license by AIP Publishing